Computational Study of the Flow in a Spinning and Nutating Cylinder

Thorwal Herbert* and Rihua Li†
Ohio State University, Columbus, Ohio 43210

Artillery shells with liquid payloads may experience severe flight instability owing to the moments exerted by the viscous fluid motion in a cylindrical payload container. Incorporation of these moments into flight simulations as a routine design tool requires a highly efficient code for solving the Navier-Stokes equations. We describe a spectral collocation method based on Chebyshev-Fourier-Chebyshev expansions in the radial, azimuthal, and axial direction. The method exploits the symmetries of the problem. By using a volume approach and an analytical result by Rosenblat, accurate moments are obtained in small fractions of the time required by other codes. Solutions for steady motion are presented and compared with numerical and experimental data.

Introduction

GYROS and rotating fluids often exhibit unexpected behavior. In the past, it has been recognized that spin-stabilized shells with liquid payloads can suffer dynamical instability originating from resonance with inertial waves.[1] Since this phenomenon is basically inviscid and is routinely avoided by proper design, it was surprising to observe in some cases another type of instability that is characterized by an increase in the nutation (or yaw) angle and a simultaneous loss in the spin rate. The rapid drop in spin rate is clearly a viscous phenomenon, and laboratory experiments, computational results, and field tests have meanwhile shown that this instability is caused by the nutation-induced fluid motion in a certain range of relatively small Reynolds numbers. Although in special cases this instability has been overcome by trial and error, the future design of reliable projectiles would profit from the opportunity to calculate the liquid moments and to account for these moments in flight simulations. The empirical data base[2] is sparse, however, and the computational methods in use[3-6] are rather demanding. An evaluation and verification of the codes by Vaughn et al.[4] and Strikwerda and Nagel[5] are currently being conducted by BRL.[7] Typical computer times for a single case are in the range of 6–12 hr on VAX-class machines. Six-degree-of-freedom flight simulations[8] typically use 2×10^5 time steps over the flight time of the order of 30 s. The study of the interaction of the interior fluid motion with the exterior aeroballistics consequently requires either a very fast subroutine for calculating the liquid moments or interpolation in a multidimensional table of 500–1000[8] precalculated values. Hence, flight simulations for liquid-filled shells are currently a very expensive tool and are not ready for routine applications.

In previous work,[9] we conducted a theoretical analysis that aimed at the origin of the viscous despin (negative roll) moment in cylinders of large aspect ratio. This analysis showed that the deviation from solid-body rotation is governed by a small parameter, $\varepsilon = (\Omega/\omega)\sin\theta$, involving the nutation rate Ω, the nutation angle θ, and the spin rate ω. A solution of the linearized equations was developed for a finite-length segment of an infinitely long cylinder, i.e., disregarding the end walls of the cylinder. The velocity field and viscous components of the moments were obtained in closed form. The velocity field consists only of an axial component of order $O(\varepsilon)$ that is the prominent feature of the fluid motion in slender cylinders and produces a negative roll moment of order $O(\varepsilon^2)$ owing to Coriolis forces. Although this roll moment is in reasonable agreement with experimental and computational data, the original analysis accounted only for the viscous part of the yaw and pitch moments. These latter moments contain essential contributions of the pressure[4] that originate from the turning of the flow near the end walls and were not captured by linear analysis. The effect of nonlinearity was studied[10] by using perturbation expansions in ε and was found to be small except for an aperiodic streaming term in the azimuthal direction.

The perturbation approach provided valuable insight into the structure of equations and solution. The analytical work suggests the use of a numerical method that exploits 1) the near-linearity of the governing equations and 2) the smoothness of the solution in the relevant range of Reynolds numbers. We have therefore pursued a simple concept that is open to further refinements. We use Chebyshev–Fourier–Chebyshev expansions in r, ϕ, and z, respectively, and convert the nonlinear equations into an algebraic system for the expansion coefficients. Linearization can be performed about the trivial solution or any other known solution, e.g., at neighboring parameters. The solution of the linear algebraic system is used as an initial approximation for iterative improvement by the modified Newton method. The feasibility of this approach has been demonstrated[11] with a crude spectral approximation to the solution. Problems in calculating the pressure that can arise from the invalidity of the basic equations along the joint of the flat end walls to the cylindrical side wall have meanwhile been overcome.[12] The present version of the code exploits the diametral symmetry of the flow about the center of the cylinder and allows for higher resolution at modest CPU times. This version can also be adapted for the analysis of unsteady problems. A dramatic increase in efficiency has recently been achieved[13] by combining an analytical result of Rosenblat et al.[6] with a volume formulation for calculating the liquid moments. The moments can be obtained from only the simply periodic components of the axial velocity and the azimuthal streaming term. A fast subroutine for flight simulations exploits the analytical results. For more accurate studies, complete tables of moments can be calculated in a few hours on an engineering workstation.

Governing Equations

We consider the steady motion of a fluid of density ρ and viscosity μ in a cylinder of radius a and length $2c$ in an

Presented as Paper 87-1445 at the AIAA 19th Fluid Dynamics, Plasma Dynamics, and Lasers Conference, June 8-10, 1987, Honolulu, HI; received Jan. 27, 1988; revision received Oct. 26, 1989.

*Professor, Departments of Mechanical Engineering and Aeronautical and Astronautical Engineering. Member AIAA.
†Research Associate, Department of Mechanical Engineering.

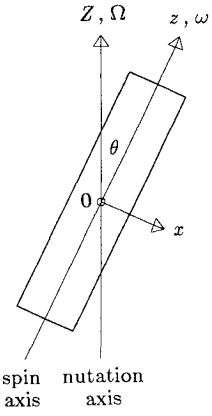

Fig. 1 Definition sketch.

aeroballistic coordinate system x,y,z, where z is the axis of the cylinder, as shown in Fig. 1. The inertial axis Z in flight direction and the z axis enclose the nutation angle θ. The cylinder rotates with the spin rate ω about z, whereas the x,z plane rotates with the nutation rate Ω about the Z axis. ω and Ω are constant. All quantities are made nondimensional using a, ω, and ρ for scaling length, time, and mass, respectively. The solution depends on four nondimensional parameters: aspect ratio $\eta = c/a$, nutation angle θ, frequency $\tau = \Omega/\omega$, and Reynolds number $Re = \rho\omega a^2/\mu$. The aspect ratio enters the solution only through the boundary conditions at the end walls of the cylinder. The motion is subject to the no-slip and no-penetration conditions at the cylinder walls. Since the velocity field degenerates for either $\omega = 0, \Omega = 0, \theta = 0$, or $\mu \to \infty$ to rigid-body rotation of the fluid, it is appropriate to concentrate on the deviation $\boldsymbol{v}^d$ of the velocity from rigid-body rotation

$$\boldsymbol{v} = \boldsymbol{v}^r + \boldsymbol{v}^d, \qquad \boldsymbol{v}^r = r\boldsymbol{e}_\phi \tag{1a, 1b}$$

where $\boldsymbol{e}_\phi$ is the azimuthal unit vector. The boundary conditions on $\boldsymbol{v}^d$ are homogeneous. The pressure field is split according to

$$p = p^r + p^d, \qquad p^r = \frac{1}{2}[r^2(1+\tau_z)^2 + r^2\tau_\phi^2 + z^2\varepsilon^2] - rz\tau_r\tau_z \tag{2a, 2b}$$

where $\tau_r = -\varepsilon\cos\phi$, $\tau_\phi = \varepsilon\sin\phi$, $\tau_z = \tau\cos\theta$, $\varepsilon = \tau\sin\theta$. The pressure p^r differs from the pressure in rigid-body rotation. The form of p^r is chosen such that a force term appears only in the z-momentum equation.

In cylindrical coordinates r,ϕ,z, the equations for the velocity components $\boldsymbol{v}^d = (v_r, v_\phi, v_z)$ and pressure p^d take the form

$$\frac{1}{r}\frac{\partial}{\partial r}(rv_r) + \frac{1}{r}\frac{\partial v_\phi}{\partial\phi} + \frac{\partial v_z}{\partial z} = 0 \tag{3a}$$

$$D'v_r - \frac{v_\phi^2}{r} - 2(1+\tau_z)v_\phi + 2\tau_\phi v_z = -\frac{\partial p^d}{\partial r} + \frac{1}{Re}\left(D''v_r - \frac{v_r}{r^2} - \frac{2}{r^2}\frac{\partial v_\phi}{\partial\phi}\right) \tag{3b}$$

$$D'v_\phi + \frac{v_r v_\phi}{r} + 2(1+\tau_z)v_r - 2\tau_r v_z = -\frac{1}{r}\frac{\partial p^d}{\partial\phi} + \frac{1}{Re}\left(D''v_\phi - \frac{v_\phi}{r^2} + \frac{2}{r^2}\frac{\partial v_r}{\partial\phi}\right) \tag{3c}$$

$$D'v_z + 2\tau_r v_\phi - 2\tau_\phi v_r = -\frac{\partial p^d}{\partial z} - 2r\tau_r + \frac{1}{Re}D''v_z \tag{3d}$$

where

$$D' = \frac{\partial}{\partial t} + \frac{\partial}{\partial\phi} + v_r\frac{\partial}{\partial r} + \frac{v_\phi}{r}\frac{\partial}{\partial\phi} + v_z\frac{\partial}{\partial z}$$

$$D'' = \frac{\partial^2}{\partial r^2} + \frac{1}{r}\frac{\partial}{\partial r} + \frac{1}{r^2}\frac{\partial^2}{\partial\phi^2} + \frac{\partial^2}{\partial z^2}$$

The primary effect of nutation is the ϕ-periodic force term $-2r\tau_r = 2\varepsilon r\cos\phi$ in the z-momentum equation (3d). For $\varepsilon = 0$, Eqs. (3) have the trivial solution $\boldsymbol{v}^d \equiv 0$, $p^d \equiv 0$. The system supports the following symmetries:

$$v_r(r,\phi+\pi,-z) = v_r(r,\phi,z), \qquad v_\phi(r,\phi+\pi,-z) = v_\phi(r,\phi,z) \tag{4a, b}$$

$$v_z(r,\phi+\pi,-z) = -v_z(r,\phi,z), \qquad p^d(r,\phi+\pi,-z) = p^d(r,\phi,z) \tag{4c, d}$$

Therefore, it is sufficient to obtain a solution in the half-cylinder, $z \geq 0$, with appropriate symmetry conditions at $z = 0$.

Some Analytical Results

The steady flow in a relatively long cylinder (aspect ratio $\eta > 4$) at a low Reynolds number is expected to exhibit little axial variation over most of the cylinder length. Previous work[9] has therefore relaxed the boundary conditions at the end walls and studied the steady flow in a finite segment of an infinitely long cylinder.

In the physical situations of interest, $\varepsilon = (\Omega/\omega)\sin\theta$ is a small parameter, and consequently, it is reasonable to pursue a perturbation expansion in ε. This provides $\boldsymbol{v}^d$ in the form

$$\boldsymbol{v}^d = \sum_{n=1}^{\infty} \varepsilon^n \boldsymbol{v}^{(n)}(r,\phi) \tag{5}$$

and similar expressions for p^d. The development of expressions for the expansion coefficients $\boldsymbol{v}^{(n)}$ from Eqs. (3) leads to an alternating pattern

$$\boldsymbol{v}^{(n)} = \begin{cases} [0,0,v_z^{(n)}], & n \text{ odd} \\ [v_r^{(n)}, v_\phi^{(n)}, 0], & n \text{ even} \end{cases} \tag{6}$$

and the components of $\boldsymbol{v}^{(n)}$ take the form

$$v_r^{(n)} = \sum_{m=1}^{n/2} (u_{nm}e^{i2m\phi} + \tilde{u}_{nm}e^{-i2m\phi}) \tag{7a}$$

$$v_\phi^{(n)} = v_{no} + \sum_{m=1}^{n/2} (v_{nm}e^{i2m\phi} + \tilde{v}_{nm}e^{-i2m\phi}) \tag{7b}$$

$$v_z^{(n)} = \sum_{m=1}^{(n+1)/2} [w_{nm}e^{i(2m-1)\phi} + \tilde{w}_{nm}e^{-i(2m-1)\phi}] \tag{7c}$$

where the tilde denotes the complex conjugate. The aperiodic term in $v_r^{(n)}$ is suppressed by the continuity equation. The r-dependent coefficient functions in Eqs. (7) are required to satisfy homogeneous boundary conditions at $r = 1$ and to be finite at the axis $r = 0$.

The axial velocity at order $O(\varepsilon)$ can be found in analytical form

$$w_{11}(r) = i\left[\frac{I_1(\alpha r)}{I_1(\alpha)} - r\right] \tag{8}$$

where I_1 denotes the modified Bessel function, and $\alpha = (1+i)(Re/2)^{1/2}$. This solution is valid for arbitrary Reynolds number but may be unstable as Re exceeds some critical value. This component is the dominating feature of the flow in a long cylinder. The interesting properties of the associated flowfield are discussed by Herbert.[9]

At order $O(\epsilon^2)$, a comparison of the equation for v_{20} with

the imaginary part of the equation for w_{11} immediately shows that the aperiodic component of the azimuthal velocity is

$$v_{20}(r) = -2Im[w_{11}(r)] \tag{9}$$

The ϕ-periodic components are governed by a coupled set of inhomogeneous differential equations with variable coefficients. With some effort, the radial velocity component of $O(\varepsilon^2)$ can be found in closed form.[10] In view of the effort involved in deriving the analytical result and the ultimate need to determine certain coefficients numerically, the differential equations for the third-order components were solved by means of a spectral collocation method.

The motion is governed by the axial component w_{11} at order $O(\varepsilon)$. Of the higher-order terms, only the aperiodic term v_{20} is substantial. In the cylinder's center section, these terms are in good agreement with computational results. All the other terms are not only of order $O(1)$ but are in fact less than unity, assuring rapid convergence of the perturbation series. The contribution of w_{31} to the despin moment is negligible. The ϕ-periodic terms oscillate about zero as r varies between $0 \le r \le 1$. The accurate representation of single high-order terms by a radial Chebyshev series may require numerous expansion functions. For the total velocity field, however, the error in representing these terms is of little importance. At Reynolds numbers in the range of maximum despin moment, reasonably accurate approximations can be obtained with only a few polynomials in the radial direction. In the azimuthal direction, the solution is governed by terms periodic in ϕ and by the aperiodic term v_{20}. Fourier series with three or five modes, therefore, provide approximations of sufficient accuracy for practical purposes. The perturbation analysis clearly shows that the main features of the flow are governed by the linear $O(\varepsilon)$ part of Eqs. (3) with small corrections for nonlinearity. This property will not change for a finite-length cylinder.

Spectral Approximations

The results of the analytical work suggest that a good approximation to the flow in a finite cylinder can be obtained by solving linearized versions of Eqs. (3). Linearization can be performed in different ways. The first is a linearization in ε. Besides Eqs. (4), the resulting equations support the additional symmetries

$$v^d(r,\phi+\pi,z) = -v^d(r,\phi,z), \quad p^d(r,\phi+\pi,z) = -p^d(r,\phi,z) \tag{10a, 10b}$$

These relations permit useful checks on the results of the spectral code. A second linear system can be obtained by linearization in the components of $\boldsymbol{v}^d$. This linearization retains coupling terms such as $2\tau_\phi v_z$ in Eq. (3b) that destroy the symmetries (10). The second system can be considered a special case with $\hat{\boldsymbol{v}}^d = 0$ of a linearization about some known solution $\hat{\boldsymbol{v}}^d$. The latter procedure is very efficient if the solution is sought for a densely spaced sequence of parameter combinations as in flight simulations.

The algebraic form of the equations is obtained by the use of spectral collocation. The velocity components are expressed in the form

$$v_r = \sum_{k=1}^{K} \sum_{l=1}^{L} \sum_{m=1}^{M} u_{klm} R^u_{kl}(r) F_l(\phi) Z^u_{ml}\left(\frac{z}{\eta}\right) \tag{11}$$

with similar expressions for v_ϕ, v_z, and p^d. The azimuthal functions are

$$F_l = \begin{cases} \cos\dfrac{l-1}{2}\phi, & l \text{ odd} \\ \sin\dfrac{l}{2}\phi, & l \text{ even} \end{cases} \tag{12}$$

The azimuthal collocation points are equidistant

$$\phi_l = 2\pi(l-1)/L, \qquad l = 1,2,\ldots,L \tag{13}$$

and L is odd.

In a first version of the code, radial and axial collocation points are located at the maxima of the highest Chebyshev polynomials (Gauss-Lobatto points). The boundary conditions are implemented by replacing three of the four differential equations in the boundary points. The question then is which equation should be retained and where the condition on the pressure, e.g., $p^d = 0$, should be applied. Trial and error leads to numerous cases with ill-determined matrices or a zero determinant. In other cases, a correct solution for the velocity field is obtained, but the pressure contains a nonphysical spurious term. The spurious term vanishes in all collocation points except the corners, where it may assume arbitrary values. Problems with spectral calculations of the pressure in closed domains with corners are well-known, but the reports on their origin and methods for solution are rather unspecific. A detailed analysis reveals that spurious terms can be systematically suppressed by retaining in the corners one of the momentum equations that contain the derivative of the pressure in the direction of the boundary.

In a second and final version of the spectral code, the problems of the pressure calculation have been avoided by using a different set of collocation points (Gauss points). The expansion functions in the radial and axial direction depend on the index l and may be different for the variables v_r, v_ϕ, v_z, and p^d. They are combinations of even or odd Chebyshev polynomials such that 1) the homogeneous boundary conditions are implicitly satisfied, 2) the symmetry conditions (4) are satisfied, and 3) the limit value of the variables for $r \to 0$ (i.e., the value on the axis) is independent of ϕ. The collocation points are

$$r_k = \sin\frac{2k-1}{4K}\pi, \qquad k = 1,2,\ldots,K \tag{14a}$$

$$\frac{z_m}{\eta} = \sin\frac{2m-1}{4M}\pi, \qquad m = 1,2,\ldots,M \tag{14b}$$

Since $0 < r_k$, no points are located on the axis. Also, $r_k < 1$, $z_m < \eta$, such that no points are located on the surface. The points in the radial and axial direction are concentrated near the boundary such that high resolution in this region is obtained without additional coordinate stretching. Thus, the boundary layers forming at higher Reynolds number can be resolved by slightly increasing K and M.

The spectral collocation method converts the linear system of partial differential equations derived from Eqs. (3) into an algebraic system of dimension $N = 4 \cdot K \cdot L \cdot M$ for the coefficients u_{klm}, v_{klm}, w_{klm}, and p_{klm} of v_r, v_ϕ, v_z, and p^d, respectively. The linear system for the expansion coefficients is solved by Gauss elimination with partial pivoting. The subroutine used retains all data required to solve the same system with a new right-hand side without repeating the costly reduction of the matrix to upper triangular form. Once the solution is obtained, a new right-hand side is formed taking the nonlinear terms into account and the system is iteratively solved until sufficient accuracy is achieved. The procedure is equivalent to the modified Newton iteration (without updating the Jacobian in every step) and converges rapidly since the nonlinear corrections to the velocity are small while the pressure appears linear in Eqs. (3).

Results for Velocity and Pressure

In the following, we present some results for the velocity and pressure fields at $\theta = 20$ deg, $\tau = 0.16667$, and $\eta = 4.368$ that result in $\varepsilon = 0.057$. The results are for $K = 6$, $L = 5$, and $M = 8$, and consequently, $N = 960$. The calculation of a

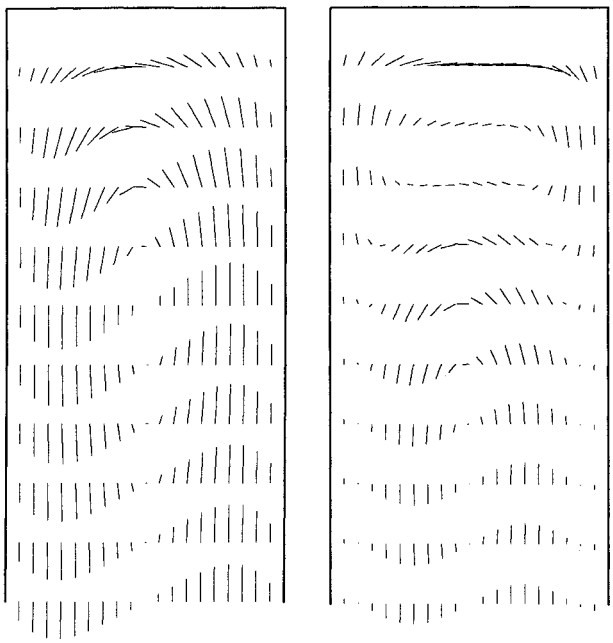

Fig. 2 Vector plot of the axial and radial velocities in the planes $\phi = 45$ deg (left, scale 0.075) and $\phi = 135$ deg (right, scale 0.0375) at $Re = 20$ for $z \geq 0$.

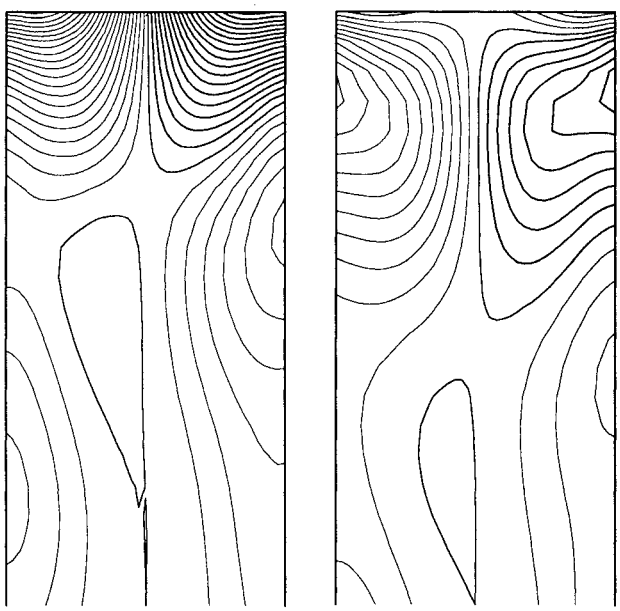

Fig. 3 Contour plot of the pressure field in the planes $\phi = 45$ deg (left) and $\phi = 135$ deg (right) at $Re = 20$ for $z \geq 0$. Levels every 0.0025.

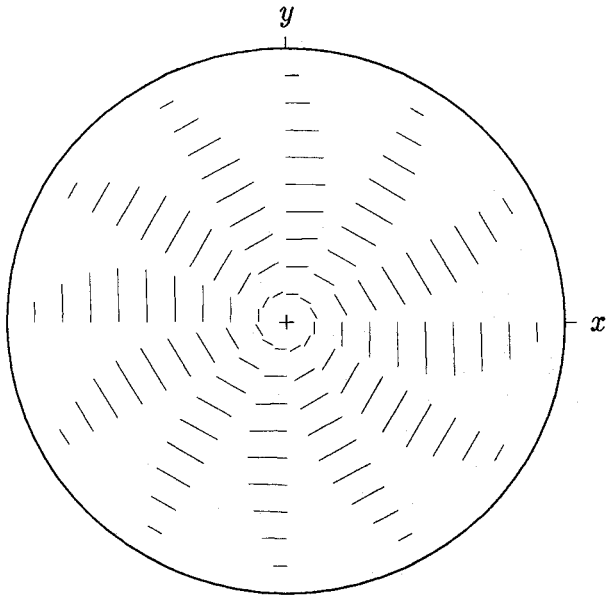

Fig. 4 Vector plot of the azimuthal velocity v_ϕ in the center plane at $z = 0$, $Re = 20$. Scale 0.003.

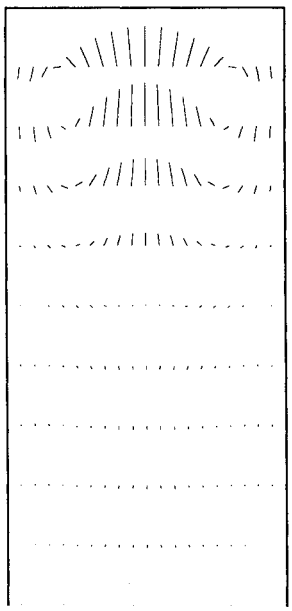

Fig. 5 Vector plot of the axial and radial mean velocity v_ϕ for $Re = 20$. Scale 0.002.

single solution with this resolution requires about 2 min on a Cray-1S. Figure 2 shows the axial and radial velocities in the planes $\phi = 45$ deg and $\phi = 135$ deg at $Re = 20$. Only the upper half, $z \geq 0$, of the cylinder is shown; the lower half is governed by the symmetries (4). The scale values give the velocity per unit length where the diameter is four units. The velocity distribution at $z = 0$ agrees well with the results of the perturbation analysis and computations with the Sandia code.[3] Near the end walls, the solution is more realistic and more accurate than the Sandia results. The figure also verifies the existence of a predominantly axial flow over most of the cylinder length, except within a region of the order of the radius near the end wall. Linear and nonlinear velocity distributions are hardly distinguishable. Clearly visible is the turning of the flow near the end wall. Although the flow appears steady in the coordinate system chosen, the velocity field describes, in fact, an oscillatory motion of fluid elements about the near-circular orbit.

The pressure distributions for the same case are shown in Fig. 3 with the heavy lines indicating positive values. Remarkable is the formation of regions of high and low pressure in the corner near $\phi \approx 45$ deg and $\phi \approx 135$ deg, respectively, that produce large contributions to the moments about the x and y axes. Except in this region near the end walls, the variation of the pressure is relatively weak. The azimuthal position of the pressure extremum changes from $\phi = 0$ for small values of Re to $\phi = 90$ deg as $Re \to \infty$.

The dominant components of velocity and pressure fields are azimuthally periodic with period 2π. The harmonics are small, indicating the small effect of nonlinearity in the range

of low Reynolds numbers. The only important nonlinear term is the aperiodic mean flow. This is clearly shown by Fig. 4 that gives the azimuthal velocity in the center plane $z = 0$. The aperiodic component is opposite to the rigid-body rotation and exerts a negative roll moment through the wall-shear stress $\tau_{r\phi}$. The axial and radial mean velocity field is given in Fig. 5. This streaming term exhibits a toroidal motion near the end in each half of the cylinder and causes a slow drift of fluid elements with respect to circular orbits. This mean velocity produces the symmetric pattern in flow visualizations[14] at low Reynolds numbers.

At the higher Reynolds number $Re = 300$, the maximum axial velocity appears at $\phi \approx 90$ deg. As shown in Fig. 6, the flow in the plane $\phi = 90$ deg breaks up into two swirls, one in each half of the cylinder, with little flow across the plane $z = 0$. Three weak swirls develop in the plane $\phi = 0$ such that the velocity field is reminiscent of a chain with five links. Notably, the breakup into cells is restricted to an inner region of the cylinder. The motion in the pronounced boundary layer visible in the plane $\phi = 0$ does not follow the cellular structure and may have a direction opposite to the core flow. The pressure variation is characteristically different from that at a low Reynolds number. Figure 7 shows the strong variation and formation of an almost symmetric pattern along the cylinder in the plane $\phi = 0$, whereas the variation at $\phi = 90$ deg is rather weak. This pressure field explains the void observations of Miller[15] that show a wavy distortion of the void in the plane $\phi = 0$ at high Reynolds numbers. The free surface in these observations can be interpreted as a surface of constant total pressure. The steep and opposite pressure gradients across the cylinder axis near $z/\eta = 0.25$ and $z/\eta = 0.75$ displace the void near these positions in opposite directions along the diameter at $\phi \approx -15$ deg as shown in Fig. 8.

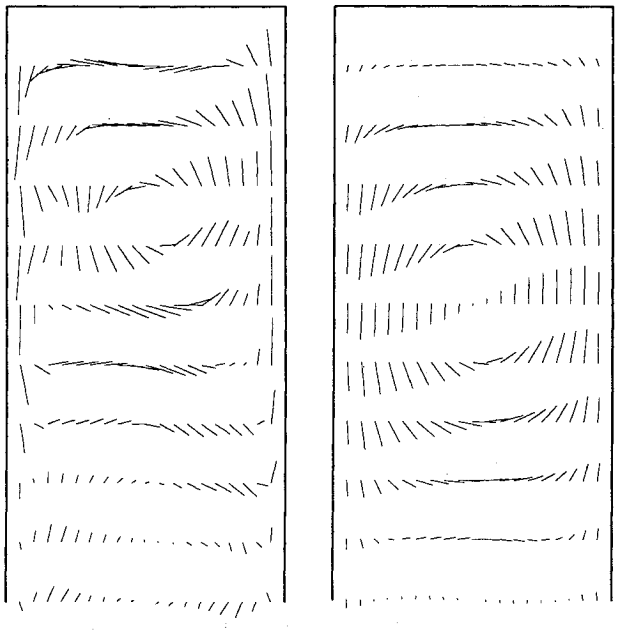

Fig. 6 Vector plot of the axial and radial velocities in the planes $\phi = 0$ deg (left, scale 0.05) and $\phi = 90$ deg (right, scale 0.2) at $Re = 300$ for $z \geq 0$.

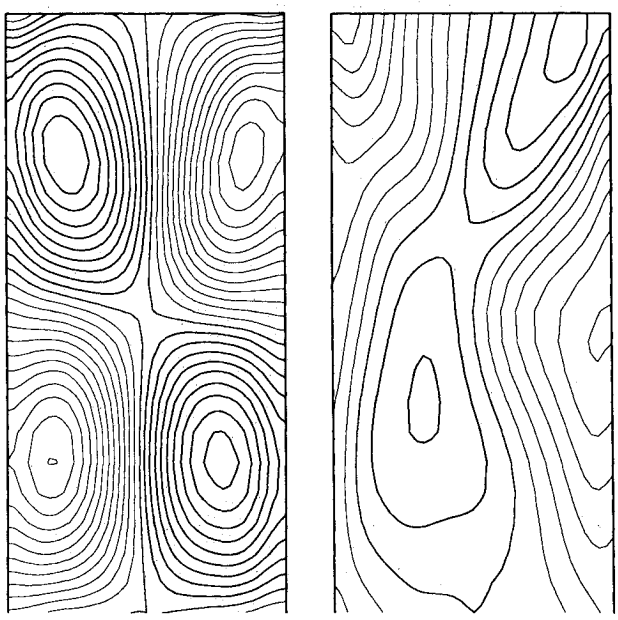

Fig. 7 Contour plot of the pressure field in the planes $\phi = 0$ deg (left) and $\phi = 90$ deg (right) at $Re = 300$ for $z \geq 0$. Levels every 0.005.

Quantitative measurements of the flow variables are available only for the pressure at different radial positions at the end walls for either very high (too high for direct Navier–Stokes solution) or very low Reynolds numbers. The measurements were made at a small nutation angle of $\theta = 2$ deg such that nonlinear effects are negligible. Figure 9 compares the results of the spectral code with the experimental data of Hepner et al.[16] and numerical results of the spatial eigenfunction method of Hall et al.[17] reported in Ref. 16. Hepner et al. use the inertial spin rate $\omega + \Omega\cos\theta$ for reference and define the pressure coefficient as

$$C_p = \frac{\Delta\tilde{p}}{\theta\rho a^2(\omega + \Omega\cos\theta)^2} \tag{15}$$

where $\Delta\tilde{p}$ is the amplitude of the pressure fluctuation recorded by a transducer at $r = 0.667$. Although the Reynolds number in their notation is fixed at $Re' = 3.1$, it varies in our notation with τ or $\tau' = \tau/(1 + \tau_z)$. Figure 9 shows good agreement of the numerical results. The minute differences near $\tau' = -0.4$ are likely due to using only 10 eigenfunctions in their numerical work. The origin of the deviation between the numerical and experimental data has not been revealed by Hepner et al.

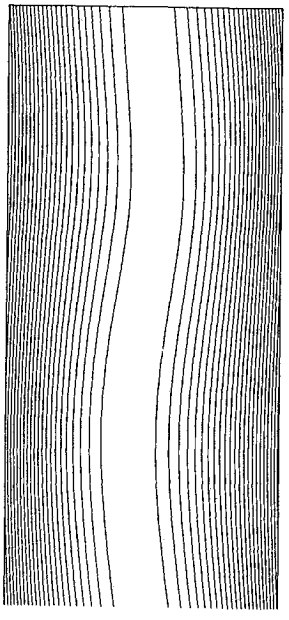

Fig. 8 Contours of constant total pressure in the plane $\phi = -15$ deg for $Re = 300$ showing the characteristic wavy distortion near the axis as the void observations of Miller (Ref. 15). Levels every 0.03.

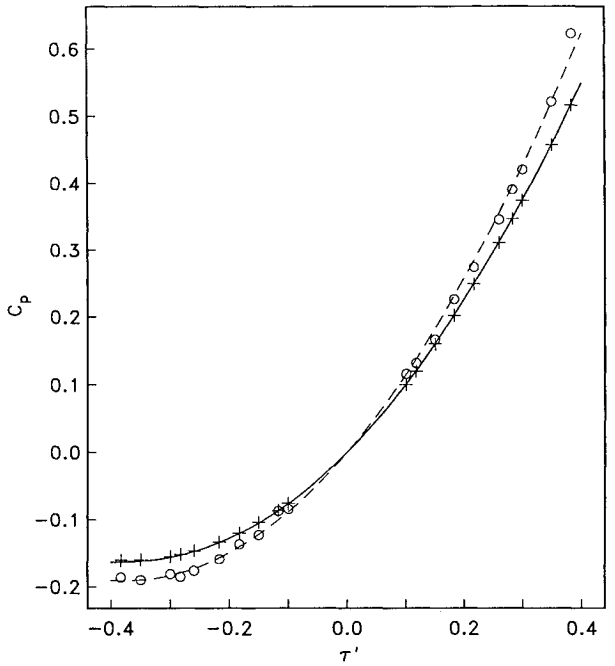

Fig. 9 Pressure coefficients C_p as a function of the nutation rate $\tau' = \tau/(1+\tau_z)$ and $Re = 3.1/(1+\tau_z)^2$. Results of the spectral code (solid line), numerical results (+) of Hall et al. (Ref. 16), experimental data (○) of Hepner et al. (Ref. 16), and approximation $C_p = 1.017\tau' + 1.355\tau'^2$ (dashed line).

Hepner et al. observe "a nonlinear dependence upon τ', resembling the leading edge of a resonant response curve." The form of this curve is clearly revealed in our analysis. To within a small change of less than $\pm 1.5\%$ caused by the variation in Re, the pressure p^d owing to the internal fluid motion is proportional to $\varepsilon = \tau \sin\theta \approx \tau\theta$ and assumes an extremum near $\phi = 0$. Equation (2b) provides the pressure amplitude at $\phi = 0$ as $p' \approx r\eta\tau^2\theta$. Therefore, C_p can be approximated as

$$C_p \approx c_1\tau' + c_2\tau'^2, \qquad c_1, c_2 = \text{const.} \tag{16}$$

as shown by the dashed line in Fig. 9.

Calculation of the Liquid Moments

The conservation of angular momentum for the steady flow in a control volume V with surface S rotating with constant rate Ω about a fixed axis requires

$$\boldsymbol{M} = \int_S (\boldsymbol{r} \times \boldsymbol{F})\, \mathrm{d}S = \int_V \boldsymbol{r} \times (2\boldsymbol{\Omega} \times \boldsymbol{v})\rho\, \mathrm{d}V + \int_V \boldsymbol{r} \times [\boldsymbol{\Omega} \times (\boldsymbol{\Omega} \times \boldsymbol{r})]\rho\, \mathrm{d}V + \int_S (\boldsymbol{r} \times \boldsymbol{v})\rho(\boldsymbol{v} \cdot \mathrm{d}\boldsymbol{S}) \tag{17}$$

where the velocity $\boldsymbol{v}$ is measured relative to the aeroballistic frame. On the left-hand side, $\boldsymbol{M}$ is the resultant torque on the control volume, $\boldsymbol{r}$ the position vector, and $\boldsymbol{F}$ the stress acting on the cylinder. The presence and meaning of certain terms depend on the choice of the control volume. The surface integral on the right-hand side of Eq. (17) vanishes if the surface of the control volume is closed.

For ease of practical application, we express the moment $\boldsymbol{M} = (M_x, M_y, M_z)$ in terms of Cartesian components that provide yaw, pitch, and roll moment, respectively. As an analogue to Eq. (1), we decompose the moments into

$$\boldsymbol{M} = \boldsymbol{M}^r + \boldsymbol{M}^d \tag{18}$$

where $\boldsymbol{M}^r$ corresponds to the pure rigid-body motion, whereas $\boldsymbol{M}^d$ originates from the deviation velocity and pressure. For the cylindrical control volume, the rigid-body rotation causes only a pitch component

$$M_y^r = 2\pi\varepsilon\eta\left[1 + \frac{\varepsilon}{\tan\theta}\left(\frac{1}{2} - \frac{2}{3}\eta^2\right)\right] \tag{19}$$

whereas $M_x^r = M_z^r = 0$. Note that $\boldsymbol{M}$ is dimensionless; the reference moment is $\rho a^5\omega^2$.

The evaluation of the components of $\boldsymbol{M}^d$ bears some ambiguity that can be exploited for advantages. Previous computational work[3-6] employed a control volume consisting of an "empty" closed cylinder with only the pressure and stresses acting on the inside surface. In this case, the right-hand side of Eq. (17) vanishes and the moments are obtained from the stresses $\boldsymbol{F}$ at the inside wall of the control volume. Here, we use a different choice that bears great advantages especially for computational work.

We consider a control volume consisting of a solid cylindrical surface completely enclosing the liquid. The moment calculation for this "full" control volume rests on the relation

$$\boldsymbol{M}^d = \int_V \boldsymbol{r} \times (2\boldsymbol{\Omega} \times \boldsymbol{v}^d)\rho\, \mathrm{d}V \tag{20}$$

Using analytical relations derived by Rosenblat et al.,[6] we can show that the components $\boldsymbol{M}^d$ take the form

$$M_x^d = -I_1 \cos\theta \tag{21a}$$

$$M_y^d = I_2 \sin\theta - I_3 \cos\theta \tag{21b}$$

$$M_z^d = I_4 \sin\theta \tag{21c}$$

where

$$I_1 = -I_4 = \int_V z(v_r \cos\phi - v_\phi \sin\phi) r\, \mathrm{d}r\, \mathrm{d}\phi\, \mathrm{d}z \tag{22a}$$

$$I_2 = \frac{1}{2}\int_V v_\phi r^2\, \mathrm{d}r\, \mathrm{d}\phi\, \mathrm{d}z \tag{22b}$$

$$I_3 = -\int_V v_z \sin\phi r^2\, \mathrm{d}r\, \mathrm{d}\phi\, \mathrm{d}z \tag{22c}$$

Finally, we obtain the moments in the form

$$M_x^d = \frac{2\varepsilon}{\tan\theta}\int_{-\eta}^{\eta}\int_0^{2\pi}\int_0^1 v_z r^2 \cos\phi\, \mathrm{d}r\, \mathrm{d}\phi\, \mathrm{d}z \tag{23a}$$

$$M_y^d = \varepsilon\int_{-\eta}^{\eta}\int_0^{2\pi}\int_0^1 v_\phi r^2\, \mathrm{d}r\, \mathrm{d}\phi\, \mathrm{d}z + \frac{2\varepsilon}{\tan\theta}\int_{-\eta}^{\eta}\int_0^{2\pi}\int_0^1 v_z r^2 \sin\phi\, \mathrm{d}r\, \mathrm{d}\phi\, \mathrm{d}z \tag{23b}$$

$$M_z^d = M_x^d \tan\theta \tag{23c}$$

The volume integral approach thus leads to handy expressions that involve only the radial and azimuthal velocity components. Integration over $\mathrm{d}\phi$ reduces the requirements, in fact, to the knowledge of the aperiodic component of v_ϕ and the simply periodic components of v_z. Therefore, the volume approach can also be applied to the analytical results just given and provides yaw and pitch moments without explicit knowledge of the pressure.

Results for the Liquid Moments

While velocity and pressure fields are primarily of basic fluid mechanical interest, the practical need for the moments dictates the measure for efficiency of the code. The moments derived from the volume approach and the surface approach

Table 1 Volume approach for the moments at $\eta = 4.368$, $\tau = 0.1667$, $\theta = 20$, $Re = 20$

K	L	M	M_x	M_y	M_z
3	3	3	0.08305	0.07475	0.03023
4	3	4	0.08260	0.07334	0.03006
5	3	5	0.08300	0.07332	0.03021
5	3	6	0.08317	0.07353	0.03027
6	3	5	0.08300	0.07332	0.03021
6	3	6	0.08317	0.07353	0.03207
4	5	4	0.08280	0.07353	0.03014
5	5	5	0.08322	0.07355	0.03029
6	5	6	0.08340	0.07374	0.03035
6	5	8	0.08335	0.07385	0.03034

Table 2 Surface approach for the moments at $\eta = 4.368$, $\tau = 0.1667$, $\theta = 20$, $Re = 20$

K	L	M	M_x	M_y	M_z
3	3	3	0.07394	0.09396	0.03308
4	3	4	0.07247	0.08133	0.02992
5	3	5	0.07904	0.07291	0.03024
5	3	6	0.08178	0.07039	0.03028
6	3	5	0.07864	0.07354	0.03023
6	3	6	0.08137	0.07115	0.03027
4	5	4	0.07289	0.08354	0.02999
5	5	5	0.07894	0.07700	0.03032
6	5	6	0.08152	0.07491	0.03036
6	5	8	0.08289	0.07415	0.03034

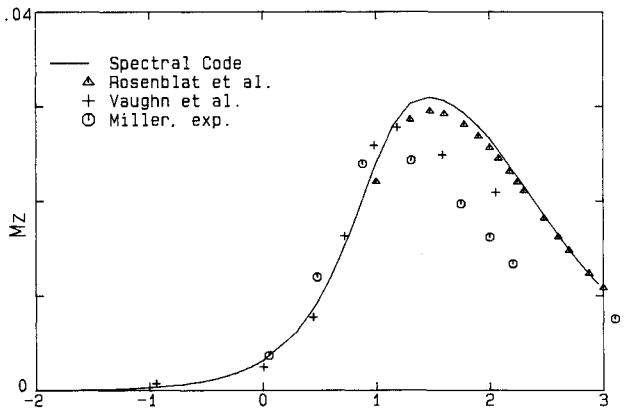

Fig. 10 Roll moment M_z vs Reynolds number Re for $\eta = 4.368$, $\tau = 0.16667$, and $\theta = 20$ deg. Comparison with numerical and experimental data.

applied to the same spectral solutions are shown in Tables 1 and 2, respectively. The Reynolds number $Re = 20$ is in the range of maximum despin moment M_z.

It is obvious that the volume approach provides results of superior quality and more rapid convergence. The required (absolute) accuracy of 10^{-3} for engineering applications can be achieved with the low truncation $K = 4$, $L = 3$, $M = 4$. This accuracy has to be seen in the light of considerable uncertainty in the moments governing the exterior aerodynamics of the projectile. As a rule of thumb, an increase in the aspect ratio requires additional expansion functions in the axial direction, whereas increasing the Reynolds number requires higher resolution in both the radial and axial directions.

Figure 10 compares the calculated roll moments for a wide range of Reynolds numbers with the experimental results of Miller[2] and with computational results.[4,6] The deviation of

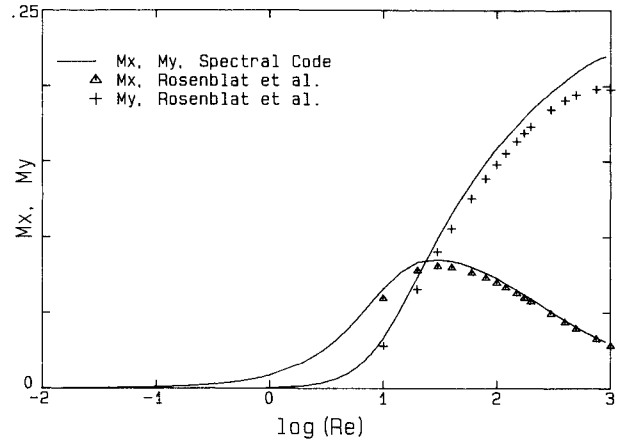

Fig. 11 Yaw moment M_x and pitch moment M_y vs Reynolds number Re for $\eta = 4.368$, $\tau = 0.16667$, and $\theta = 20$ deg. Comparison with numerical data.

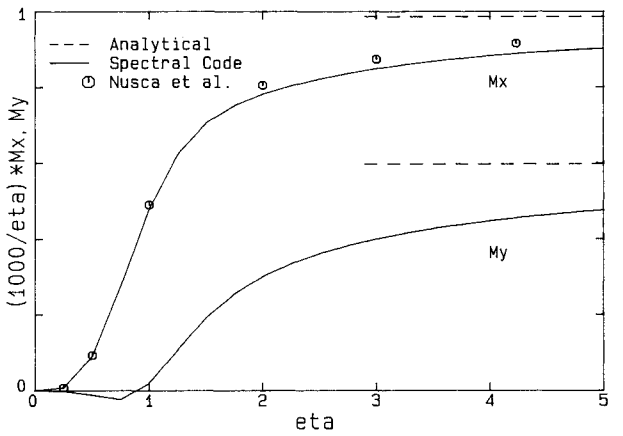

Fig. 12 Yaw moment M_x and pitch moment M_y per unit length vs aspect ratio η at $Re = 10$, $\tau = 0.16667$, and $\theta = 2$ deg. Comparison of present numerical results with analytical results for $\eta \to \infty$ and data obtained by Nusca with Strikwerda's code.

the results of the Sandia code[4] is caused by using inappropriate formulas for the moments in the nutating coordinate system.[7] The agreement with the other computational data is good. Test runs with high resolution suggest that the small difference from the results of Rosenblat et al.[6] is due to the lower resolution of the finite-element code in combination with the application of the surface approach for the moments. The experiments were made in a range of spin rates ω between 2000 and 4000 rpm. Although $\omega = 3000$ rpm has been used in Fig. 10, the assumption of a lower value would improve the comparison with respect to the maximum values.

Figure 11 shows a similar comparison for the yaw and pitch moments. The results of the Sandia code are suppressed since they suffer from a dimensional inconsistency.[7] Although the agreement for the yaw moment at high Reynolds numbers is surprisingly good, the deviation in the pitch moment is likely to originate from insufficient resolution of the steep pressure gradients. This effect of discretization errors has been reduced in the spectral code by using the volume approach for calculating the moments.

Figure 12 shows the dependence of the yaw and pitch moments per unit length (the roll moment is proportional to M_x) on the aspect ratio of the cylinder and compares with results of the code written by Strikwerda and Nagel[5,7] and the analytical results for $\eta \to \infty$. This diagram indicates that a reduction in the overall liquid moments for a given fluid mass can be achieved by splitting the cylindrical volume into slices of low aspect ratio.

Discussion

The codes previously in use may serve for establishing some basic results but are to inefficient for routine applications. The finite-difference code developed at Sandia Laboratories[3,4] rests on Chorin's method of artificial compressibility and provides the steady solution at $11 \times 24 \times 21$ grid points in the r,ϕ,z direction by integrating over typically 10^4 to 8×10^4 time steps, a task that requires 6 to 48 min of CPU time on a Cray-1S. The result consists of over 22,000 values of the velocities v_r, v_ϕ, v_z and the pressure p at the grid points.

Strikwerda and Nagel[5] briefly describe a code using finite differences in the radial and axial direction and pseudospectral differencing in the azimuthal direction. Nonuniform grids are introduced for increased resolution near the walls. The difference equations are solved by an iterative method based on successive overrelaxation. The computer time required is comparable to that of the Sandia code. A thorough evaluation of the two codes is currently being conducted at BRL.[7]

The experience with the present version of the spectral code shows that high performance can be achieved. The solution is obtained in semianalytical form with only $N = 4 \cdot K \cdot L \cdot M$ (typically less than 500) numerical coefficients. This low data volume is especially attractive for storage and for communication with remote supercomputers. The code is very well suited for vectorization, since practically all CPU time is spent on constructing and solving an algebraic system. The code demands larger memory than other codes, because 64-bit arithmetic is highly recommended for spectral methods in general, and the algebraic system requires $N(N+1)$ words of storage. A run with $N = 500$ requires about 2 Mbyte of memory and can easily be carried out on engineering workstations within a few minutes, whereas moment calculations with $N = 192$ are a matter of seconds. Since the memory requirement is acceptable even if higher resolution is desired, the method applied here is a viable alternative in numerous other fluid mechanical problems. The ability to obtain accurate solutions for the steady problem directly from (large) algebraic systems bears valuable potential to answer the question whether the steady solution is stable and allows the analysis of unsteady motions with implicit time stepping. The design of a reliable code for the unsteady problem can profit from the knowledge of the eigenvalue spectrum for small unsteady disturbances of the steady flow.

Although the calculation of velocity and pressure fields provides insight into the physics of the flow, the practical interest in the moments for the quasisteadily changing parameters in flight simulations can be satisfied with modest amounts of computer time. This is due to using a modified Newton method that updates the Jacobian only when demanded by deteriorating convergence.

In general, the volume approach provides much more accurate results than the surface approach. This improvement is due to the additional smoothing of fluctuating data by integrating over three instead of two space directions and to using fewer, less fluctuating, and more accurate input data. The absence of v_r in the volume formulation is welcome. This velocity component is small over most of the cylinder length but is oscillatory in the radial direction[10] with considerable gradients near the wall. Near the end walls, v_r is of the same order as v_z with steep gradients toward the end wall. Inspection of the velocity plots of Vaughn et al.[4] indicates that these gradients were difficult to resolve by the finite-difference method. The aperiodic component of v_ϕ is a relatively small streaming term of smooth and almost uniform behavior along the cylinder axis. The large azimuthally periodic components of v_ϕ near the end walls do not affect the moment calculation.

Probably the greatest advantage of the volume formulation is the absence of pressure from the moment equations. This property favors the use of pressure-free sets of basic equations, e.g., in terms of vorticity or vector potential. The smaller number of dependent variables can be exploited for further increasing the efficiency. Even in natural variable formulations, the pressure is difficult to obtain with high accuracy because of the invalidity of the equations in the joints of the flat end walls to the cylindrical side wall. As shown in Fig. 3, the pressure may assume extrema near the corners and, therefore, inaccuracies in this region may strongly influence yaw and pitch moment. In this context, it is instructive to evaluate the convergence history of the artificially time-dependent method implemented in the Sandia code.[3] Whereas the velocity rapidly reaches a quasisteady state, about 75% of the iterations are spent on improving the pressure field. We estimate that by the use of the volume approach, equivalent or superior values for the moments could be obtained with less than 20% of the iterations. It is worthwhile to note that the analytical results of Rosenblat et al.[6] and Eqs. (21) and (22) for the moments are valid for closed containers of a more general shape and thus can be used for other interior flow problems.

Our analytical and numerical tools allow quick estimates and efficient calculation of accurate liquid moments. These results also suggest guidelines for the suppression of the flight instability caused by the viscous-liquid payload. For a given cavity and fluid, a reduction in the overall liquid moments can be achieved in two ways. The first method is the split of the cylindrical volume into slices of low aspect ratio. The second way is the longitudinal split into k^2 "straws" of high aspect ratio $k\eta$. The change of radius reduces the Reynolds number; this may or may not be desirable. The nondimensional moment per straw increases due to the increasing aspect ratio. An essential reduction of the overall moments, however, originates from the fact that the dimensional moments are proportional to the fifth power of the radius. The dimensional factor is therefore reduced by k^{-5} per straw or k^{-3} for all straws together. As a raw estimate, the effective moments can be reduced by a factor k^{-2}.

Acknowledgments

We greatly appreciate fruitful discussions with M. C. Miller, S. Rosenblat, and M. Nusca, and the availability of their results prior to publication. This work is supported by the U.S. Army AMCCOM under Contract DAAA15-85-K-0012. Part of the computations have been performed with the Cray-XMP/28 of the Ohio Supercomputer Center.

References

[1]Sedney, R., "A Survey of the Fluid Dynamic Aspects of Liquid-Filled Projectiles," AIAA Paper 85-1822-CP, 1985.

[2]Miller, M. C., "Flight Instabilities of Spinning Projectiles Having Nonrigid Payloads," *Journal of Guidance, Control, and Dynamics*, Vol 5, 1982, pp. 151–157.

[3]Vaughn, H. R., Oberkampf, W. L., and Wolfe, W. P., "Numerical Solution for a Spinning Nutating Fluid-Filled Cylinder," Sandia Rept. SAND 83-1789, Albuquerque, NM, 1983.

[4]Vaughn, H. R., Oberkampf, W. L., and Wolfe, W. P., "Fluid Motion Inside a Spinning Nutating Cylinder," *Journal Fluid Mechanics*, Vol. 150, 1985, pp. 121–138.

[5]Strikwerda, J. C., and Nagel, Y. M., "A Numerical Method for Computing the Flow in Rotating and Coning Fluid-Filled Cylinders," in *Proceedings 1984 Scientific Conference on Chemical Defense Research*, edited by M. Rausa, CRDC-SP-85006, Albuquerque, NM, 1985, pp. 523–527.

[6]Rosenblat, S., Gooding, A., and Engleman, M. S., "Finite-Element Calculations of Viscoelastic Fluid Flow in a Spinning and Nutating Cylinder," Rept. CRDEC-CR-87021, Chemical Res. Dev. and Eng. Ctr. Aberdeen Proving Ground, MD, 1986.

[7]Nusca, M. J., and D'Amico W. P., "Parametric Study of Low Reynolds Number Precessing/Spinning Incompressible Flow," Memo. Rept. BRL-MR-3657, Ballistic Res. Lab., 1988.

[8]Vaughn, H. R., Wolfe, W. P., and Oberkampf W. L., "Six Degree of Freedom Simulation of Fluid Payload Projectiles Using Numerically Computed Fluid Moments," Sandia Rept. SAND 85-1166, Albuquerque, NM, 1985.

[9]Herbert, T., "Viscous Fluid Motion in a Spinning and Nutating Cylinder," *Journal of Fluid Mechanics*, Vol. 167, 1986, pp. 181–198.

[10]Herbert, T., Li, R., and Greco, S. D., "Perturbation Analysis of the Viscous Flow in a Spinning and Nutating Cylinder of Large Aspect Ratio," *Physics of Fluids* (in preparation).

[11]Herbert, T., "Analytical and Computational Studies of the Fluid Motion in Liquid-Filled Shells," in *1986 Proceedings of 4th Army Conference on Applied Mathematics and Computing*, ARO Rept. 87-1, Army Research Office, Research Triangle Park, NC, 1987, pp. 627–636.

[12]Herbert, T., "A Spectral Navier–Stokes Solver for the Flow in a Spinning and Nutating Cylinder," in *Proceedings of 1986 Scientific Conference on Chemical Defense Research*, edited by M. Rausa, CRDC-SP-87005, Chemical Res. Dev. and Eng. Center, Aberdeen Proving Ground, MD, 1987, pp. 455–460.

[13]Li, R., and Herbert, T., "Calculation of the Liquid Moments in a Spinning and Nutating Cylinder," *Journal of Guidance, Control and Dynamics* (in preparation).

[14]Herbert, T., and Pierpont, D., "Visualization of the Flow in a Spinning and Nutating Cylinder," in *Proceedings of 1985 Scientific Conference on Chemical Defense Research*, edited by M. Rausa, CRDC-SP-86007, Chemical Res. Dev. and Eng. Center, Aberdeen Proving Ground, MD, 1986, pp. 989–994.

[15]Miller, M. C., "Void Characteristics of a Liquid Filled Cylinder Undergoing Spinning and Nutating Motion," *Journal of Spacecraft and Rockets*, Vol. 18, 1981, pp. 286–288.

[16]Hepner, D. J., Soencksen, K. P., Davis, B. S., and Maiorana, N. G., "Internal Pressure Measurements for a Liquid Payload at Low Reynolds Numbers," Memo. Rept. BRL-MR-3674, Ballistic Res. Lab., 1988.

[17]Hall, P., Sedney, R., and Gerber, N., "Fluid Motion in a Spinning, Coning Cylinder via Spatial Eigenfunction Expansion," Tech. Rept. BRL-TR-2813, Ballistic Res. Lab., Aberdeen Proving Ground, MD, 1987.